

# Titanium Nitride Microelectrode: A New Candidate for In Situ Electrochemical Transmission Electron Microscopy Study

Junbeom Park, Ningyan Cheng, Binghui Ge, Eva Jodat, André Karl, Yevheniy Pivak, Hongyu Sun,\* Héctor Hugo Pérez Garza,\* Shibabrata Basak,\* and Rüdiger-A. Eichel

In situ transmission electron microscopy (TEM) is increasingly utilized by researchers to explore various electrochemical applications in the quest to address climate change, aiming to comprehend underlying mechanisms and enhance performance. However, the conventional Pt microelectrode commonly used in in situ TEM poses limitations due to its low electron transparency and high catalytic activity. In this study, titanium nitride ( $\text{TiN}_x$ ) is introduced as a novel microelectrode material that can be fabricated following typical cleanroom processes. Through in situ Zn and Cu electrodeposition studies, it is shown how the low catalytic activity and higher electron transparency of  $\text{TiN}_x$  enable obtaining stable electrochemical cycling and quantify the deposition on top of microelectrode in TEM mode, highlighting the benefit of  $\text{TiN}_x$  microelectrodes for different in situ TEM studies.

## 1. Introduction

Electrochemistry is a crucial technology for energy storage and conversion, e.g., battery, fuel cell, electrolysis, etc., offering potential solutions to the global energy crisis and climate change.<sup>[1,2]</sup> For instance, transitioning to electric vehicles can reduce the greenhouse gas emissions from road transport sector by 11.9%.<sup>[3]</sup> Additionally, electrochemical recycling of carbon dioxide can further lead to net-zero carbon economy.<sup>[4,5]</sup> As electrochemistry involves interactions between electrons and ions, nanoscale investigations are necessary to understand fundamental mechanisms and improve application performances.


In situ transmission electron microscopy (in situ TEM) allows the characterization of morphological, crystallographic, and chemical information at the nanoscale with various stimuli such as heat,<sup>[6,7]</sup> electricity,<sup>[8,9]</sup> at various gas,<sup>[10,11]</sup> and liquid environments.<sup>[12,13]</sup> Many in situ TEM studies related to energy materials have already been reported.<sup>[14,15]</sup> The microelectromechanical-system (MEMS)-based chips enable creation of working environment, mimicking real-world scenarios, around the sample reliably with minimal drift.<sup>[16,17]</sup> Platinum (Pt) microelectrodes are widely used in MEMS chips for electrical biasing because of their good electrical conductivity, chemical stability, and fabrication availability through comparatively clean room processes.<sup>[18]</sup> However, using Pt microelectrodes for electrochemistry can restrict the proper understanding of underlying mechanisms for two reasons. First, Pt itself is a well-known electrochemical catalyst, so Pt microelectrodes can react to the electrochemical environment additionally from the planned reaction.<sup>[19]</sup> For example, a Pt microelectrode with an aqueous solution can lead to a hydrogen evolution reaction.<sup>[20]</sup> Therefore, an alternative microelectrode is crucial for a better understanding of electrochemical reactions. Second, the high atomic number of the Pt microelectrode results in low electron transparency. As the electrochemical reaction occurs around the microelectrode, only results that occur at the edge (i.e., outside of the microelectrode) are clearly visible in TEM mode.<sup>[21]</sup> Although scanning TEM (STEM) mode is more conducive to detecting deposition on top of the Pt microelectrode, the typical scan rate of conventional STEM detectors (<5 frames per second, fps) is not high enough to observe fast

J. Park, E. Jodat, A. Karl, S. Basak, R.-A. Eichel  
Institute of Energy and Climate Research – Fundamental Electrochemistry (IEK-9)  
Forschungszentrum Jülich GmbH, Jülich 52425, Germany  
E-mail: s.basak@fz-juelich.de

N. Cheng, B. Ge  
Information Materials and Intelligent Sensing Laboratory of Anhui Province  
Key Laboratory of Structure and Functional Regulation of Hybrid Materials of Ministry of Education  
Institutes of Physical Science and Information Technology  
Anhui University  
Hefei 230601, China

Y. Pivak, H. Sun, H. H. P. Garza  
DENSolutions B.V.  
Informaticalaan 12, ZD Delft 2628, The Netherlands  
E-mail: hongyu.sun@densolutions.com;  
hugo.perez@densolutions.com

S. Basak  
Ernst Ruska-Centre for Microscopy and Spectroscopy with Electrons and Peter Grünberg Institute  
Forschungszentrum Jülich GmbH, Jülich 52425, Germany

 The ORCID identification number(s) for the author(s) of this article can be found under <https://doi.org/10.1002/adem.202302146>.

© 2024 The Authors. Advanced Engineering Materials published by Wiley-VCH GmbH. This is an open access article under the terms of the Creative Commons Attribution License, which permits use, distribution and reproduction in any medium, provided the original work is properly cited.

DOI: 10.1002/adem.202302146

electrochemical reactions compared to the scan rate of TEM ( $>100$  fps).

Glassy carbon is one potential alternative to Pt microelectrodes.<sup>[22,23]</sup> However, analytical analysis of carbon-based material on top of glassy carbon microelectrode may be challenging. Hence, a non-carbon-based alternative microelectrode material should be developed. This article proposes a ceramic titanium nitride ( $\text{TiN}_x$ ) as a solution. For this, the working, counter, and reference  $\text{TiN}_x$  microelectrodes are fabricated using a simple reactive magnetron sputtering technique that is coherent with the MEMS device fabrication workflow. The MEMS chips containing  $\text{TiN}_x$  microelectrodes were tested at a liquid-biasing in situ TEM setup (Figure S1, Supporting Information).<sup>[24]</sup> The behavior of the conventional Pt microelectrode and that of the new  $\text{TiN}_x$  microelectrode during Zn electroplating are compared. Furthermore, the electroplating and stripping behaviors of Cu occurring on top of our  $\text{TiN}_x$  microelectrode are investigated. This study offers a new microelectrode material for studying electrochemistry in TEM, which can lead to a more thorough understanding of this field and potentially contribute to the fast improvement of electrochemical storage and conversion devices.

## 2. Results and Discussion

The  $\text{TiN}_x$  microelectrodes were fabricated with rectangular and round shapes in a periodical arrangement as can be seen in **Figure 1**. The surface area of a single  $\text{TiN}_x$  microelectrode on SiN window is around  $8 \times 5 \mu\text{m}$  with  $3 \mu\text{m}$  diameter hole. The scanning electron microscopy energy-dispersive X-Ray spectroscopy (SEM-EDS) elemental mapping showed the fabricated structure of  $\text{TiN}_x$  microelectrode on the Si MEMS chip (Figure S2, Supporting Information). All the mapping results match well with the MEMS chip design (Figure S2h, Supporting Information). The small amount of oxygen was detected due to the absorbed water or surface oxidation.

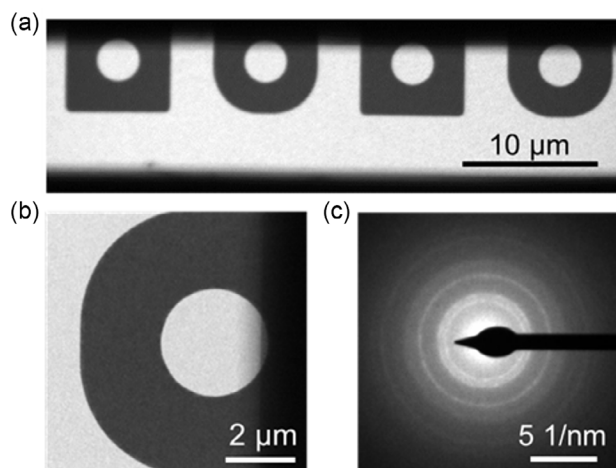


**Figure 1.** a,b) The  $\text{TiN}_x$  microelectrodes at different magnifications and c) a typical SAED pattern obtained from round-shaped  $\text{TiN}_x$  microelectrode.

### 2.1. Comparison of Pt and $\text{TiN}_x$ Microelectrode during Electrochemical Plating and Stripping Behaviors of Zn

In principle, an ideal microelectrode to perform electrochemical experiments should allow the proposed biasing stimuli and prevent side reactions. To compare the behavior of Pt and  $\text{TiN}_x$  microelectrode during electrochemical processes, cyclic voltammetry (CV) between  $-1.5$  and  $+1.0$  V at scan rate  $100 \text{ mVs}^{-1}$  was performed with  $100 \text{ mM ZnSO}_4$  aqueous solution separately. With Pt microelectrode, there are many spikes and fluctuations in the obtained CV curves (**Figure 2a**). Moreover, bubble formation was observed on microelectrode as highlighted by the arrow in **Figure 2b**. These results indicate the applied voltage on the Pt microelectrode not only plated and stripped Zn but also formed gas bubbles from the solution. As Pt has a low hydrogen evolution potential, the formed bubble from the working microelectrode would be hydrogen gas. As the gas evolution reaction from aqueous solution with Pt microelectrode is hard to avoid, the results could not purely represent the target electrochemistry. Additionally, the formed bubble pushed the liquid and led to contact loss between liquid and working microelectrode, which would explain the origin of spikes and fluctuation in CV (**Figure 2a**). Notably, with the  $\text{TiN}_x$  microelectrode, smooth and continuous CV curves were obtained (**Figure 2c**) without bubble formation during CV scanning (**Figure 2d**). Thus, as opposed to the results obtained with the Pt microelectrode, the applied bias on the  $\text{TiN}_x$  microelectrode might be fully used to plate and strip the Zn without any side reactions, confirming that the  $\text{TiN}_x$  microelectrodes are well-suited candidates for electrochemical experiments. To show the long-term stability of the  $\text{TiN}_x$  microelectrode, we have performed a 50 cycle CV

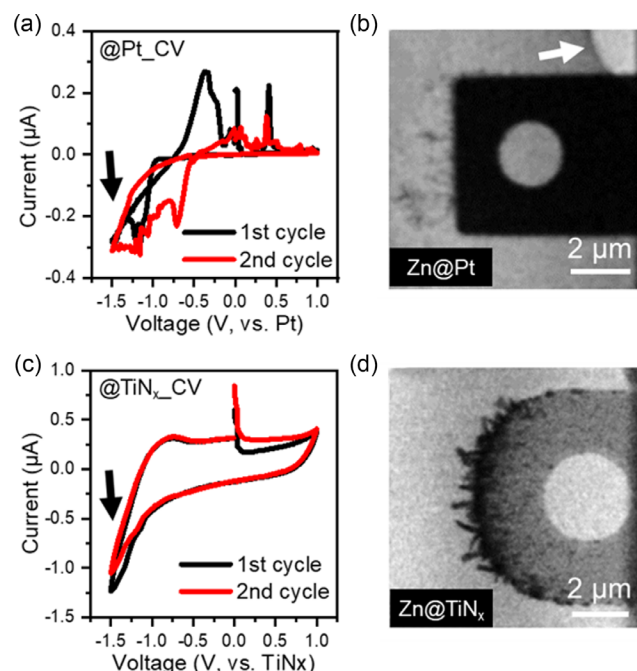


**Figure 2.** Cyclic voltammetry curves and TEM images acquired while performing Zn plating and stripping on a,b) Pt and c,d)  $\text{TiN}_x$  microelectrode, respectively.

(Figure S3, Supporting Information) ex situ and TEM investigations are carried out after 11th, 21st, and 50th cycle. TEM investigation reflects that the microelectrode remains intact after this long-term cycling. It should be pointed out that the gradual decrease of the current with increasing cycles during the last 30 CV cycles (Figure S3c, Supporting Information) is related to the increasing amount of detached Zn particles during cycling (and thus could not be stripped electrochemically during CV), as can be seen in Figure S3f, Supporting Information.

Electrochemical reaction stability is an essential factor, but visibility is also a critical factor for in-depth in situ TEM electrochemical studies. As electron beam cannot easily transmit the Pt microelectrode (typically around 70 nm thickness used) due to high atomic number, plated Zn could be recognized only at the outside of the Pt microelectrode (Figure 2b). However, plated Zn was fully visible all around and on top of the  $\text{TiN}_x$  microelectrode (Figure 2d). Additionally, low-magnification TEM image proved that Zn plating was evenly performed on whole  $\text{TiN}_x$  microelectrodes (Figure S4a, Supporting Information). The selected area electron diffraction (SAED) pattern of plated Zn on  $\text{TiN}_x$  microelectrode (Figure S4b,c, Supporting Information) was bright and sharp enough to be analyzed after subtracting the SAED pattern of pure  $\text{TiN}_x$  microelectrode (Figure 1b). Therefore, compared to Pt,  $\text{TiN}_x$  can solve not only reaction stability but also TEM visibility, which leads to in-depth investigation even when the deposition occurs on top of the microelectrode.

## 2.2. Investigation of Electrochemical Plating and Stripping Behaviors of Cu on Top of $\text{TiN}_x$ Microelectrode

Cu is one of important electrocatalysts for the electrochemical reduction of  $\text{CO}_2$ . The nanostructure of Cu such as the exposed

facets or the surface atom arrangements affects not only the activity but also the product selectivity. To investigate Cu plating and stripping behavior on  $\text{TiN}_x$  microelectrode via TEM imaging, four-cycle chronoamperometry (CA) (between +1.5 and -1.5 V) was performed in the mixture aqueous solution of 20 mM  $\text{CuSO}_4$  and 10 mM  $\text{KH}_2\text{PO}_4$  (Figure S5, Supporting Information). The complete process can be followed via Movie S1, Supporting Information. The whole process can be divided into four plating phases (P1–P4) and three stripping phases (S1–S3). The plating phase led to Cu deposition without any coalescence (Figure 3a–d). From P1 to P4, the size of plated Cu particles enlarged and the number of plated Cu particles decreased. The small gray features shown at the outside of  $\text{TiN}_x$  microelectrode on TEM images would be electron-beam-induced deposited Cu nanoparticles.<sup>[21]</sup>

For further quantitative analysis of each plated Cu particles (Figure 3e–h), image process was performed to all TEM images. The processing steps can be found in Figure S6 and S7, Supporting Information. Movie S1, Supporting Information, also includes the outcome of the processing. Since the experiments are performed in TEM mode, quantitative analyses are based on area rather than volume. During each plating (P1–P4), the measured Cu plated area continuously increased and the plating rate (slope) got slower along plating time (Figure 3e). During each stripping (S1–S3), the measured Cu plated area continuously decreased with a constant stripping rate (slope) (Figure 3f). The stripping rate got slower along phases. After the initial nucleation, there were no further nucleation during the individual plating phase but the number of nucleation decreased to almost half from P1 to P2 and from P2 to P4. Number of nucleation sites for the phase P2 and P3 are similar (Figure 3g). The average particle area enlarged smoothly at each plating phase after initial growth and the real growth rate increased along phases (Figure 3h). We assume that the amounts

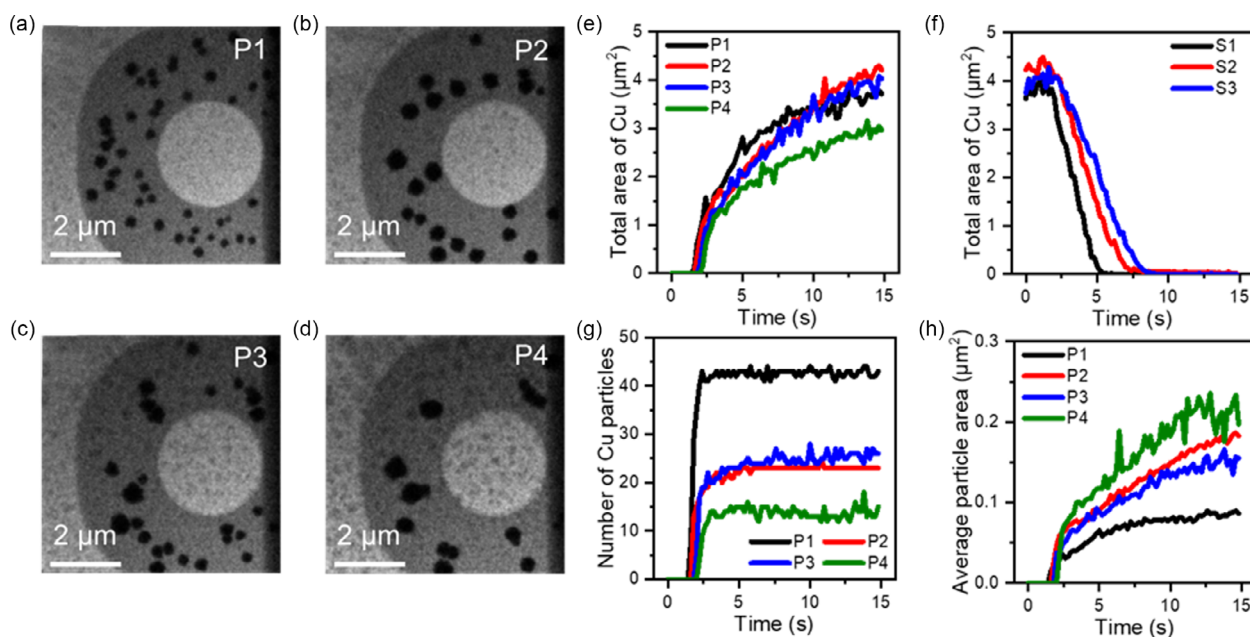


**Figure 3.** a–d) In situ TEM images of Cu plating on  $\text{TiN}_x$  microelectrode at 15 s from each plating phases. e) Total plated Cu area at each plating phases. f) Total plated Cu area at each stripping phases. g) Number of Cu particles at each plating phases. h) Average Cu particle area at each plating phases. All the tracking data were extracted from in situ TEM images by image processing (Figure S6, Supporting Information).

of plated Cu ions were similar through the phases (same current and time), the Cu ions were gathered closely and less number of larger Cu particles were formed along phases. The stripping behavior is purely affected by the surface to volume of particles and thus the stripping rate is slower for the large particles, as can be seen in Figure 3f.

### 3. Conclusion

We fabricated  $\text{TiN}_x$  microelectrodes by reactive magnetron sputtering technique and performed electroplating and stripping experiments via in situ TEM. Compared to Pt microelectrode, all electroplating and stripping of Zn with  $\text{TiN}_x$  microelectrode were stable without bubble formation and that of plated Zn were fully visible even on top of  $\text{TiN}_x$  microelectrode. Based on the high electron transparency of  $\text{TiN}_x$ , electroplating and stripping of Cu deposited on top of microelectrode were investigated and further quantification were made. These results showcase the effectiveness of  $\text{TiN}_x$  microelectrodes in achieving an in-depth understanding of electrochemical processes and encourage researchers to use  $\text{TiN}_x$  microelectrodes for liquid-phase battery,  $\text{CO}_2$  conversion, and electrolysis studies via in situ TEM.

### 4. Experimental Section

**Fabrication and Characterization of MEMS Chip with  $\text{TiN}_x$  Microelectrodes:** The titanium nitride ( $\text{TiN}_x$ ) thin film was deposited on a p-type silicon (100) substrate by reactive magnetron sputtering technique. A Ti metal target was placed at a short distance (i.e., few tens of mm) away from the substrate. The chamber was initially evacuated by a rotary pump and multiple diffusion pumps lower to  $10^{-8}$  mbar, then the chamber pressure was set to a few  $10^{-6}$  mbar with  $\text{N}_2$  gas flow. The chamber pressure was a major factor determining the conductivity and stability of  $\text{TiN}_x$  film. In general, lower pressure allowed to get not only higher conductivity but also weaker stability due to enhancing the in-plane stress. Different tests were done to maximize both conductivity and stability of  $\text{TiN}_x$  film. After the  $\text{TiN}_x$  film was successfully deposited on the substrate, standard lithography techniques and reactive ion etching were used to pattern the  $\text{TiN}_x$  microelectrodes and thus generate the final layout with the working, reference, and counter microelectrodes, which were eventually partially encapsulated with  $\text{SiN}_x$  film.

The fabricated  $\text{TiN}_x$  microelectrodes on MEMS chip were characterized by TEM (FEI Tecnai 20 D375 Twin) for morphology and crystallographic structure and SEM (Zeiss SUPRA55 SAPPHERE, 15 kV) equipped with an EDS for morphology and chemical composition.

**In Situ Electrochemical TEM Studies:** The in situ electrochemical Zn and Cu plating and stripping phenomena were studied by using a TEM holder with liquid flow and biasing function (Stream LB, DENSsolutions, Netherlands) (Figure S1, Supporting Information). The liquid cell was formed between a top and a bottom MEMS chip with an O-ring in between. Both chips had electron transparent  $\text{SiN}_x$  windows ( $\approx 50$  nm thickness) and the bottom chip was the functional chip containing the  $\text{TiN}_x$  microelectrodes. The commercially available Stream LB Nano-Cell chip with Pt microelectrodes is also used in this paper for comparison. Before the assembly, the chips were treated by oxygen plasma for 2 min to form hydrophilic surface. During the assembly, the  $\text{SiN}_x$  windows of the top and the bottom chips were aligned. After the assembled TEM holder passed the leakage test, the holder was inserted into TEM.

Two liquid solutions (for Zn plating: 100 mM  $\text{ZnSO}_4$  aqueous solution and for Cu plating: 20 mM  $\text{CuSO}_4$  with the addition of 10 mM  $\text{KH}_2\text{PO}_4$  aqueous solution) were prepared. One of the liquid solutions was flowed into the liquid cell by gas pressing system via a polyetheretherketone tubing. With a liquid flow rate of  $2\text{--}5\ \mu\text{L min}^{-1}$ , the reaching time from the

system to the liquid cell was less than 1 min. After 1 min, the liquid flow was stopped and all the experiments were done without flowing the liquid (static mode).

Electrical biasing was applied to the liquid cell by using PalmSens 4C potentiostat with  $100\ \text{mV s}^{-1}$  scan rate. Microelectrode calibration was performed with 1 mM standard ferrocenyl-methanol in 100 mM KCl aqueous solution. A droplet ( $\approx 4\ \mu\text{L}$ ) of the standard solution was placed on the bottom chip to cover the three microelectrodes, and then the CV curves were recorded. Based on the well-known characteristics of the oxidation and reduction couple, 0.0 V versus reversible hydrogen microelectrode was correlated to  $-0.45\ \text{V}$  versus  $\text{TiN}_x$ .

Electroplating and stripping of Zn was performed on both Pt and  $\text{TiN}_x$  microelectrodes with CV starting from 0, +1.0,  $-1.5$ , and back to 0 V, respectively. Electroplating and stripping of Cu was performed on the  $\text{TiN}_x$  microelectrodes with CA between +1.5 and  $-1.5\ \text{V}$  per 15 s. The plating and stripping phenomena were recorded by TEM (FEI Tecnai 20 D375 Twin, high tension: 120 kV, Emission:  $6\ \mu\text{A}$ , Spot size 5) with an Olympus Megaview G2 camera, or captured by a screen recorder software (Camtasia). After plating the Zn, the TEM holder was disassembled to perform a postmortem analysis, and thus the bottom chips were characterized by TEM.

The post-processing and quantitative image analysis for Cu plating and stripping behaviors were performed with python programming (Figure S6, Supporting Information). After the original TEM images were captured, the images were processed as: 1) crop ( $600 \times 600$  pixel around microelectrode); 2) rotate ( $4^\circ$ ); 3) Gaussian filter (noise reduction); 4) mask (removal outside of microelectrode); 5) subtraction from the reference image (pure microelectrode image, non-plated); 6) threshold (Figure S7, Supporting Information); and 7) segmentation with watershed algorithm.<sup>[25]</sup> After segmentation, the result table contained the location and area of each particle of each image, respectively. Finally, size of Cu particles during plating and stripping could be tracked based on the location data.

### Supporting Information

Supporting Information is available from the Wiley Online Library or from the author.

### Acknowledgements

J.P. and N.C. contributed equally to this work. This work is partly financed by the WBSO program of the Netherlands, which encourages firms to spend time on research and development activities. J.P. acknowledges funding provided by the Bundesministerium für Bildung und Forschung, the project iNEW FKZ 03F0589A (BMBF, German Research Foundation). E.J., A.K., and R.-A.E. acknowledge the funding provided by the BMBF (German Research Foundation) through the project DERIEL (03HY122C). N.C. acknowledges the National Natural Science Foundation of China (no. 52201003). B.G. acknowledges supports from National Natural Science Foundation of China (no. 11874394) and the University Synergy Innovation Program of Anhui Province (No. GXXT-2020-003). S.B. acknowledges "Electroscopy" (grant no. 892916) from the Marie Skłodowska-Curie action.

Open Access funding enabled and organized by Projekt DEAL.

### Conflict of Interest

Y. Pivak, H. H. P. Garza, and H. Sun work for DENSsolutions B.V., a company manufacturing and marketing in-situ TEM systems. The remaining authors have no conflicts to declare.

### Data Availability Statement

The data that support the findings of this study are available in the supplementary material of this article.



## Keywords

electrochemistry, image processings, liquid-phase transmission electron microscopies, metal plating and strippings, titanium nitride microelectrodes

Received: February 14, 2024  
Published online: April 3, 2024

- [1] R. Schlögl, *ChemSusChem* **2010**, 3, 209.
- [2] S. P. S. Badwal, S. S. Giddey, C. Munnings, A. I. Bhatt, A. F. Hollenkamp, *Front. Chem.* **2014**, 2, 79.
- [3] H. Ritchie, M. Roser, P. Rosado, Our World in Data **2020**.
- [4] S. R. Foit, I. C. Vinke, L. G. J. de Haart, R.-A. Eichel, *Angew. Chem. Int. Ed.* **2017**, 56, 5402.
- [5] A. Bagger, W. Ju, A. S. Varela, P. Strasser, J. Rossmeisl, *ChemPhysChem* **2017**, 18, 3266.
- [6] T.-H. Kim, J.-H. Bae, J.-W. Lee, K. Shin, J.-H. Lee, M.-Y. Kim, C.-W. Yang, *Appl. Microsc.* **2015**, 45, 95.
- [7] R. Schierholz, D. Kröger, H. Weinrich, M. Gehring, H. Tempel, H. Kungl, J. Mayer, R.-A. Eichel, *RSC Adv.* **2019**, 9, 6267.
- [8] M. Hammad Fawey, V. S. K. Chakravadhanula, M. A. Reddy, C. Rongeat, T. Scherer, H. Hahn, M. Fichtner, C. Kübel, *Microsc. Res. Tech.* **2016**, 79, 615.
- [9] S. Basak, A. H. Tavabi, K. Dzieciol, V. Migunov, V. Arszewska, H. Tempel, H. Kungl, E. M. Kelder, M. Wagemaker, C. George, J. Mayer, R. E. Dunin-Borkowski, R.-A. Eichel, *Chem. Commun.* **2022**, 58, 3130.
- [10] E. D. Boyes, P. L. Gai, C. R. Phys. **2014**, 15, 200.
- [11] T. Yokosawa, T. Alan, G. Pandraud, B. Dam, H. Zandbergen, *Ultramicroscopy* **2012**, 112, 47.
- [12] M. R. Hauwiler, J. C. Ondry, A. P. Alivisatos, *JoVE* **2018**, 135, 57665.
- [13] A. F. Beker, H. Sun, M. Lemang, J. T. Van Omme, R. G. Spruit, M. Bremmer, S. Basak, H. H. Pérez Garza, *Nanoscale* **2020**, 12, 22192.
- [14] S. Basak, K. Dzieciol, Y. E. Durmus, H. Tempel, H. Kungl, C. George, J. Mayer, R.-A. Eichel, *Chem. Phys. Rev.* **2022**, 3, 031303.
- [15] Z. Fan, L. Zhang, D. Baumann, L. Mei, Y. Yao, X. Duan, Y. Shi, J. Huang, Y. Huang, X. Duan, *Adv. Mater.* **2019**, 31, 1900608.
- [16] L. F. Allard, W. C. Bigelow, M. Jose-Yacamán, D. P. Nackashi, J. Damiano, S. E. Mick, *Microsc. Res. Tech.* **2009**, 72, 208.
- [17] A. J. Leenheer, J. P. Sullivan, M. J. Shaw, C. T. Harris, *J. Microelectromech. Syst.* **2015**, 24, 1061.
- [18] V. Guarnieri, L. Biazzi, R. Marchiori, A. Lago, *Biomatter* **2014**, 4, e28822.
- [19] S. Sui, X. Wang, X. Zhou, Y. Su, S. Riffat, C. Liu, *J. Mater. Chem. A* **2017**, 5, 1808.
- [20] C. C. L. McCrory, S. Jung, I. M. Ferrer, S. M. Chatman, J. C. Peters, T. F. Jaramillo, *J. Am. Chem. Soc.* **2015**, 137, 4347.
- [21] N. Cheng, H. Sun, A. F. Beker, J. T. Van Omme, E. Svensson, H. Arandiyán, H. R. Lee, B. Ge, S. Basak, R. A. Eichel, Y. Pivak, Q. Xu, H. Hugo Pérez Garza, Z. Shao, *Nanotechnology* **2022**, 33, 445702.
- [22] O. J. A. Schueller, S. T. Brittain, G. M. Whitesides, *Sens. Actuators, A* **1999**, 72, 125.
- [23] W. Dachraoui, R. Pauer, C. Battaglia, R. Erni, *ACS Nano* **2023**, 17, 20434.
- [24] J. T. van Omme, H. Wu, H. Sun, A. F. Beker, M. Lemang, R. G. Spruit, S. P. Maddala, A. Rakowski, H. Friedrich, J. P. Patterson, H. H. P. Garza, *J. Mater. Chem. C* **2020**, 8, 10781.
- [25] M. Gamarra, E. Zurek, H. J. Escalante, L. Hurtado, H. San-Juan-Vergara, *Biomed. Signal Process. Control* **2019**, 53, 101575.